

Spatiotemporal variation in N₂O flux within a slope in a Japanese cedar (*Cryptomeria japonica*) forest

Kazuya Nishina · Chisato Takenaka ·
Shigehiro Ishizuka

Received: 30 December 2008 / Accepted: 23 July 2009 / Published online: 9 August 2009
© Springer Science+Business Media B.V. 2009

Abstract Topographic factors affect nitrogen cycling in forest soils, including nitrous oxide (N₂O) emissions, which contribute to the greenhouse effect. We measured the N₂O flux at 14 chambers placed along a 65-m transect on a slope for 1 year at 2- to 3-week intervals. We applied a hierarchical Bayesian model with a conditional autoregressive (CAR) model to assess the spatiotemporal N₂O flux along a slope and quantify the effects of environmental factors on N₂O emissions. N₂O fluxes at chambers located at lower positions along the slope were relatively greater than those at higher positions. During the non-soil-freezing period, N₂O fluxes fluctuated seasonally depending on soil temperature. The soil temperature dependency of N₂O fluxes at each chamber increased with descending slope position (the median of the Q₁₀ equivalent simulated from posterior distribution

ranged from 1.18 to 3.64). According to the Bayesian hierarchical model, this trend could be partially explained by the C/N ratio at each chamber position. During the soil-freezing period, relatively high N₂O fluxes were observed at lower positions along the slope.

Keywords Bayesian hierarchical model · Conditional autoregressive (CAR) · N cycle · Spatiotemporal N₂O flux · Topographic factor

Introduction

Nitrous oxide (N₂O) is the third highest emitted greenhouse gas responsible for human-induced climate change (IPCC 2001). In addition to its contribution to global warming, N₂O plays an important role in ozone depletion in the stratosphere (Crutzen 1995). Forest soils are thought to contribute about 20% of the annual N₂O emissions into the atmosphere, but estimations of forest soil emissions of N₂O are highly uncertain (IPCC 2001). This is largely because N₂O fluxes from forest soils exhibit high spatial heterogeneity even on a plot scale-level (e.g., Ishizuka et al. 2005; Konda et al. 2008). To quantify N₂O estimation more accurately, a comprehensive understanding of N₂O variations at a plot scale-level as well as factors controlling their spatial and temporal variability is required (Mosier 1998).

K. Nishina · C. Takenaka
Graduate School of Bioagricultural Sciences of Nagoya
University, Furo-cho, Chikusa-ward, Nagoya,
Aichi 464-8601, Japan

K. Nishina (✉)
Graduate School of Environment and Information
Sciences of Yokohama National University, 79-7
Mineoka-cho, Hogogaya-ward, Yokohama, Kanagawa
464-8601, Japan
e-mail: kazuya.nishina@gmail.com

S. Ishizuka
Forestry and Forest Products Research Institute, 1,
Matsunosato, Tsukuba, Ibaraki 305-8687, Japan

Recent studies suggest that in a forest ecosystem, micro-topographic factors such as slope position are highly important in determining the spatial variability of N₂O emissions given the differing oxidation status of soils (McSwiney et al. 2001; Osaka et al. 2006). These studies suggest that the highest N₂O emissions come from lower positions on the slope. Although the spatial variability of N₂O flux has been studied, the temporal (seasonal) variation of the spatial variation of N₂O flux is still poorly understood. To reduce the uncertainty of the N₂O budget, detailed simultaneous monitoring of both the spatial and temporal variability of N₂O fluctuations is needed. In addition, to clarify the phenomena of spatiotemporal variability, including the effects of environmental factors such as temperature dependency, precise empirical modeling is required (Hawkins et al. 2007).

Studies have reported highly skewed N₂O fluxes, both temporally and spatially, in various environments such as cropland, grassland, and forested areas (e.g., Velthof et al. 1996; Lark et al. 2004; Ishizuka et al. 2005). In addition, the distribution of N₂O flux both temporally and spatially appeared to follow an approximate lognormal distribution. Thus, many reports use log-transformed N₂O flux values to estimate model parameter values for statistical modeling (e.g., Davidson et al. 2004). Log-transformation can achieve linearization of the relationship between the objective (response) and explanatory (predictor) variables as well as stabilization of the model error variance, thus satisfying the assumption of equal variances. However, a log-transformed analysis induces bias even when used as a correction factor (Stow et al. 2006). A Bayesian approach can be applied to address this problem. Recently, improved processing rates of personal computers as well as free software such as WinBUGS (<http://www.mrc-bsu.cam.ac.uk/bugs/winbugs/contents.shtml>) have resulted in the availability of a Bayesian statistical model using the Markov chain Monte Carlo (MCMC) method (Spiegelhalter and Best 2000). In the Bayesian approach, similar to a generalized linear model, many probabilistic distributions are covered. Therefore, analysis of N₂O flux as a lognormal distribution using a Bayesian framework without transformation of variables is straightforward.

Using the example of denitrification rates in cropland soil, Parkin and Robinson (1989) demonstrated that the stochastic model is preferable over deterministic models for improving the prediction of a highly

skewed distribution. Bayesian statistics can more readily cope with stochastic variables and parameters, and thus a Bayesian framework is most suitable for modeling spatiotemporal N₂O fluxes. This type of approach enables quantification of the uncertainty of the prediction by presenting a credible interval (Clark 2005). Furthermore, Bayesian statistical tools can be applied for complex models such as hierarchical structures that always exist in field study (Clark 2005). The traditional model (nonspatial, single-level regression model) could not handle problems such as spatial dependence and thus would not adequately quantify the uncertainty of such parameters (Gelfand et al. 2005). As a solution to this problem, Gelfand et al. (2005) suggested that adding random spatial effects to the model enables it to cope with spatial problems.

We aimed to evaluate the spatiotemporal variability of N₂O fluxes induced by micro-topographic factors using measurements of the N₂O flux at 14 chambers sequentially located along a slope in even-aged Japanese cedar (*Cryptomeria japonica*) forest for 1 year. We used a Bayesian hierarchical linear modeling approach to analyze the spatiotemporal N₂O flux data. In this model, a conditional autoregressive (CAR) spatial random effect model was used to analyze spatially dependent data, and thus we were able to evaluate the effect of environmental factors on spatiotemporal N₂O fluxes.

Materials and methods

Site description

The study was conducted within the Nagoya University Forest (35°81'20"N, 137°83'40"E, altitude 1,010 m), Toyota, Aichi Prefecture, Japan. The site was located on a north-facing slope with a 24° incline (detail information in Nishina et al. 2009). The vegetation consisted of even-aged (35 years old) Japanese cedar trees without undergrowth. The tree density was approximately 2,000 individuals/ha and the mean tree height was 20 m. The soil type was categorized as inceptisols according to the USDA soil taxonomy (USDA/NRCS 1999). The mean annual temperature and the annual precipitation at a camp located 100 m from the study site were 10°C and 2,200 mm, respectively (2001–2004; Yoshida and Hijii 2006). The annual litterfall was approximately 5 mg dry weight

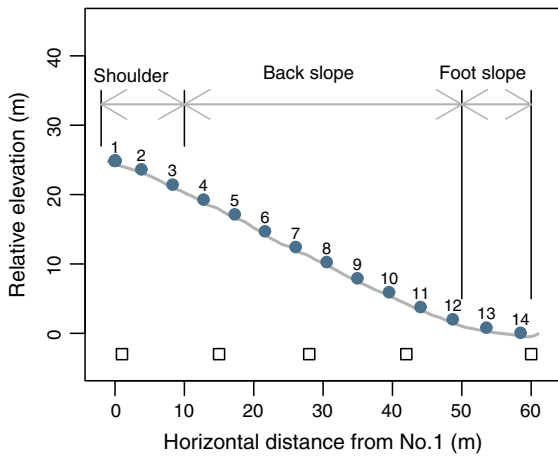


Fig. 1 The location of chambers along the transect. *Solid circles* show the location of chambers and the *numbers* indicate the chamber ID. *Open squares* show the location of frost measurements

ha⁻¹ year⁻¹ (Yoshida and Hijii 2006). During the measurement period, the maximum air temperature was 27.5°C in August and the minimum temperature was -6.8°C in March. We also measured daily throughfall precipitation (mm day⁻¹) in the plot using a rain gauge (ECRN-50; Decagon Devices, Pullman, WA).

A 65-m line transect was established along a slope from the shoulder to the bottom (Fig. 1). The elevation difference between the uppermost and lowest points was 25 m. The slope angles along the transect ranged from 5° to 36° (mean 24°, SD 8°). Fourteen chambers were set at 5-m intervals along the transect. These chambers were sequentially numbered from the top of the slope with number 1 as the uppermost chamber and 14 as the lowest. The transect was divided into three parts: shoulder, back slope, and foot slope according to Schoeneberger et al. (1998) (Fig. 1). The general properties of the soil samples that were taken after the last flux measurement on December 2007 are summarized in Table 1. The humus type of O layer was mull at the shoulder and moder at the foot slope.

N₂O flux measurement

N₂O flux was measured using a closed chamber method with a cylindrical stainless steel chamber (40 cm diameter and 15 cm height; Ishizuka et al. 2000). The chambers were inserted approximately 5 cm deep into the soil with a cutting root. Gas sampling was initiated 1 month after setting to avoid the influence of soil disturbance. A 40-ml gas sample

Table 1 General soil properties of each chamber position

Chamber ID	Physical properties of surface layer (A layer)		Thickness (cm)			pH		Carbon content (g kg ⁻¹)		Nitrogen content (g kg ⁻¹)		C:N ratio	
	Dry bulk density (Mg m ⁻³)	Solid phase ratio (%)	O layer	A layer	B layer	A layer	B layer	A layer	B layer	A layer	B layer	A layer	B layer
1	0.417	12.7	5.0	8	28	3.51	3.98	139.8	62.8	9.4	3.7	14.9	16.7
2	0.412	12.6	5.0	8	38	3.71	4.24	84.7	38.3	5.3	2.7	15.9	14.1
3	0.610	19.5	4.0	7	34	3.91	4.32	76.4	39.7	5.4	2.7	14.1	14.8
4	0.615	19.5	2.5	15	37	3.93	4.34	87.0	27.4	5.8	2.1	15.0	12.9
5	0.491	14.4	5.0	12	33	4.03	4.26	74.5	28.7	5.1	2.3	14.5	12.5
6	0.447	13.8	5.0	15	47	3.78	4.26	103.4	33.7	6.4	2.6	16.1	14.4
7	0.441	14.7	4.0	8	23	3.63	4.14	101.9	46.1	7.2	3.0	14.1	15.2
8	0.348	10.5	4.0	10	30	3.75	4.20	96.0	54.9	7.2	3.9	12.7	14.0
9	0.338	10.9	2.0	16	88	3.91	4.38	94.6	40.7	7.2	3.1	13.1	13.3
10	0.525	15.6	1.0	10	28	4.22	4.37	74.6	55.3	5.9	4.1	12.6	13.5
11	0.558	17.4	1.0	17	47	4.21	4.36	83.7	57.4	7.1	4.3	11.8	13.3
12	0.555	16.9	1.5	10	35	4.22	4.43	91.8	34.0	7.6	3.0	12.2	11.3
13	0.809	26.0	0.0	20	32	5.23	5.21	31.5	35.4	3.1	3.2	10.2	11.0
14	0.836	29.3	0.0	24	32	5.12	5.14	37.6	9.1	3.8	1.4	9.9	6.5

was taken 0, 30, and 60 min after sealing the chamber with a polyvinyl carbonate lid that was attached to an air bag to equilibrate the inside air pressure to the atmospheric pressure. Each gas sample was taken from the headspace of the chamber using a 50-ml syringe equipped with three-way cocks and a rubber septum. Gas samples were brought back to the laboratory for gas concentration measurements. The concentration of N₂O was analyzed using a gas chromatograph with a ⁶³Ni electron capture detector (GC-8A; Shimadzu, Kyoto, Japan); 5% CH₄ in argon was used as the carrier gas and N₂ was the make-up gas. N₂O fluxes (μg-N m⁻² day⁻¹) were calculated using the nonlinear model of Hutchinson and Mosier (1981) to correct for the reduction in soil gases concentration gradient with time as the gas accumulated inside the chamber. The flux measurements were conducted from December 2006 to December 2007 at 2- or 3-week intervals.

Soil temperature and soil moisture measurements

Soil temperature was measured using a thermometer (NT-250; NT Co., Tokyo, Japan) at each chamber during each sampling period. In addition, the soil volumetric water content (hereafter VWC; %) for a 12 cm depth of surface soil was measured using a handheld water content reflectometer with a 12-cm time domain reflectometry (TDR) probe (Hydro-Sense; Campbell Scientific, Logan, UT) at each chamber during each sampling. The VWC for each chamber was determined by taking seven repeated measurements near the chamber. The percentage of water-filled pore space (WFPS, %) was calculated from the VWC as well as the solid phase ratio of the soil (Danielson and Sutherland 1986). Soil frost depth was measured using the methylene blue method (Hardy et al. 2001). A PVC tube with methylene blue solution was inserted into the soil, and we defined the length of frozen dye as the frost depth.

Statistics

We incorporated a hierarchical Bayes model into the spatiotemporal model for determining N₂O flux. A Bayesian framework allowed us to cope with the spatial dependency of the data by adding a precise error structure to the model. In addition, we incorporated a CAR model to the statistical model to

account for spatial dependency. We did not incorporate the data of N₂O flux during freezing periods into the model given the unreliable mechanism for determining N₂O emissions in frozen soil.

First, we defined the likelihood of models as follows: N₂O flux (abbreviated as N_2O_{ij}) at the i th Chamber on the j th day was lognormally distributed with the scale parameter μI_{ij} and the shape parameter σI_{ij} ;

$$N_2O_{ij} \sim \log - \text{normal}(\mu I_{ij}, \sigma I_{ij}) \quad (1)$$

Given that the WFPS ($WFPS_{ij}$) and the annual mean WFPS at each chamber ($anWFPS_i$) were estimated by repeated measurements, these factors were suitable for representing a normal distribution with mean and variance, which were calculated using the measurement values.

$$WFPS_{ij} \sim \text{normal}(\mu_{WFPS}, \sigma_{WFPS_{ij}}) \quad (2)$$

$$anWFPS_i \sim \text{normal}(\mu_{anWFPS}, \sigma_{anWFPS_i}) \quad (3)$$

The descriptions of explanatory variables as a probabilistic distribution enabled us to account for their uncertainty in the inference of parameters.

Second, in a process model, the temporal mean μI was considered to be explained by soil temperature (ST_{ij}) with β_1 for each chamber, and WFPS ($WFPS_{ij}$) as well as spatially structured random intercept for the chambers ($\beta_2 ID_i$; defined as follows).

$$\mu I_{ij} = \beta_1 * ST_{ij} + \beta_2 * WFPS_{ij} + \beta_0 + \beta_2 ID_i \quad (4)$$

Third, we set up parameter models in which β_1 (or β_1) determined the soil temperature dependency of N₂O flux at the i th chamber.

$$\beta_1 \sim \text{normal}(\mu_2, \sigma_2) \quad (5)$$

We assumed that μ_2 depended on environmental factors. Previous reports suggest that the temperature dependency of N₂O emissions is controlled by soil moisture and environmental factors (Brumme 1995; Maag and Vinther 1996; Smith et al. 1998; Papen and Butterbach-Bahl 1999). Therefore, we incorporated the annual mean WFPS ($anWFPS_i$) and surface C/N ratio (CN_ID_i) as fixed effects into μ_2 .

$$\mu_2 = \alpha_1 * anWFPS_i + \alpha_2 * CN_ID_i + \alpha_0 \quad (6)$$

For $\beta_2 ID_i$, we incorporated the spatial structured random intercept for each chamber, which is referred to as an intrinsic CAR model (Besag et al. 1991). We

fit this spatial model using the “car.normal” function within WinBUGS.

$$betaID_i \sim normal(b_i, \sigma ID_i/n_i) \quad (7)$$

$$b_i = \frac{1}{n_i} \sum_{j=neighbor(i)} b_j \quad (8)$$

where n_i is the number of neighbors of neighborhood i .

Finally, we specified the hyper prior distribution for the other parameters. We used a non-informative prior for the each parameter, where all σ values were set to inverse gamma (0.001, 0.001).

We made use of MCMC methods implemented with a Bayesian inference using Gibbs' sampling software WinBUGS. For convergence diagnostics, we used Gelman Rubin's convergence diagnostic as an index. For each model, we ran the Gibbs sampler for 50,000 iterations for three chains with a thinning interval of 10 iterations. We discarded the first 25,000 iterations as burn-in and used the rest as chains to calculate posterior estimations.

For each chamber and overall chambers (plot scale), we simulated a Q_{10} equivalent as the ratio of N_2O flux at $T + 10^\circ C$ to the flux at T in $^\circ C$ ($0-10^\circ C$) from the posterior distribution of the foregoing model. Then, for the simulated data set, the WFPS at each chamber was randomly sampled from the posterior distribution of $anWFPS_i$. Soil temperature (T) was set as a sequence of integers from 0 to $10^\circ C$ ($n = 1,002$). At each soil temperature for each chamber, we determined the estimation via 1,002 simulations. In the same way, to evaluate the predictive properties of the model, we also simulated N_2O flux from the posterior distributions of the model, with the condition that soil temperature was set from 0 to $21^\circ C$ (a sequence of integers, $n = 1,002$).

Results

Soil temperature and WFPS during the measurement period

Soil temperatures ranged from approximately -1 to $21.0^\circ C$, with no substantial differences among chambers on the same sampling day during the measurement period. The soil was frozen on days 31 and 70. In these days, the forest canopy of this site had a snow cover, however, there was no snow cover on the

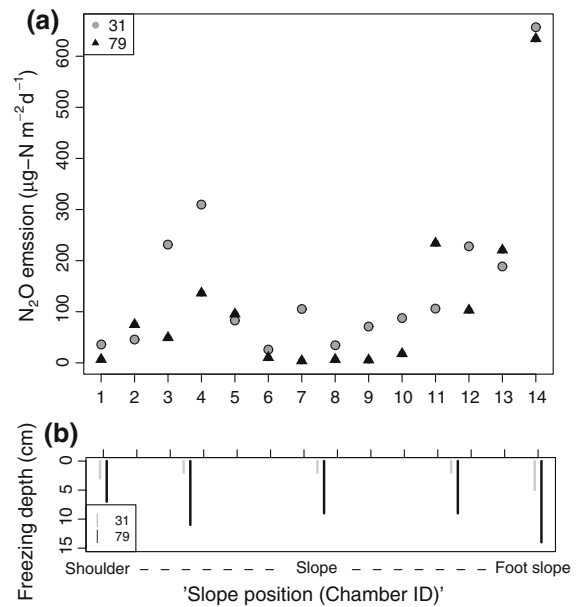


Fig. 2 Spatial variation in N_2O flux (a) and soil depth (b) during freezing periods. Circle and bar colors indicate sampling day (day of year)

ground and the chamber. The depth of soil freezing varied along the slope and it was deepest at the foot of slope on the 70th day (Fig. 2b). The mean value and range of the WFPS differed among chambers. WFPS gradually increased with descending slope. The annual mean of the WFPS at each chamber position ranged from 37.8% (Chamber 1) to 84.1% (Chamber 13). The average and standard deviation of the coefficient of variation of the WFPS at each chamber during the measurement period were 22.3 and 3.2%, respectively. The standard deviation of WFPS for each chamber on each day ($n = 7$) ranged from 0.8% to 20.2% over the entire measurement period.

N_2O flux

N_2O fluxes within all chambers for the entire measurement period ranged from 1.44 to 1,330 $\mu\text{g-N m}^{-2}\text{day}^{-1}$ (median 110 $\mu\text{g-N m}^{-2}\text{day}^{-1}$) and the distribution of N_2O fluxes was highly skewed (skewness was 2.86 and kurtosis was 16.6). The N_2O fluxes were generally greater in the summer than the winter (Fig. 3c). However, during the freezing period (on days 31 and 70), the N_2O fluxes in some chambers were relatively high (i.e., 656 $\mu\text{g-N m}^{-2}\text{day}^{-1}$ at No. 14 on the 31st day), compared to nonfreezing days in winter.

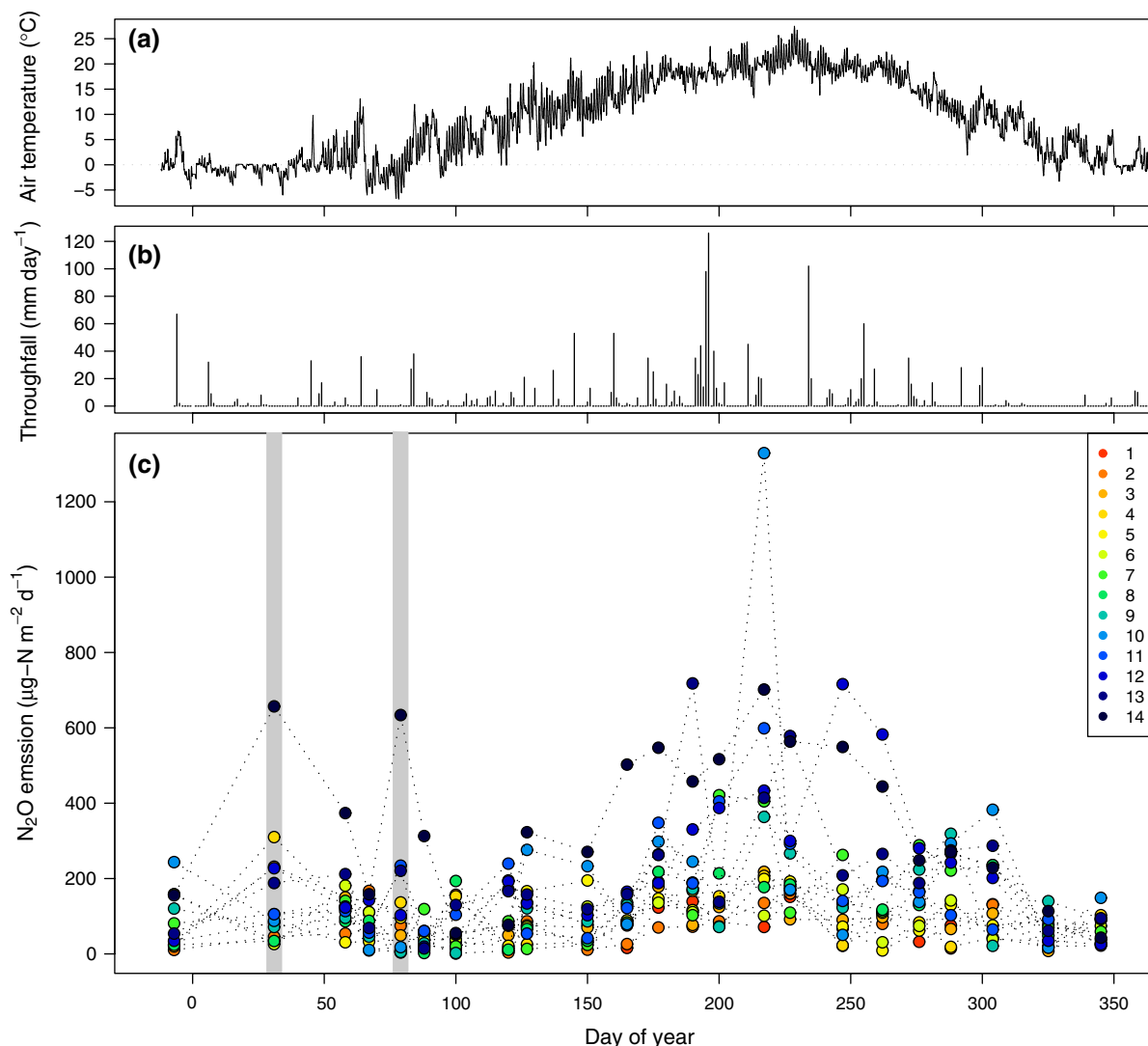


Fig. 3 Seasonal patterns of air temperature (a), daily through fall (b) and N₂O flux (c). In c shaded areas indicate the periods of soil freezing. The data for each chamber are distinguished by colored circles

When comparing the N₂O fluxes among chambers, the N₂O fluxes at the foot of the slope were relatively higher than those at the shoulder of the slope (Fig. 4). In most of the chambers, the frequency distributions of N₂O flux were skewed and the mean values were greater than the median. The median of the N₂O flux at each chamber ranged from 70.2 to 322.9 μg-N m⁻² day⁻¹. In addition, during the freezing period, the N₂O flux varied spatially and ranged from 4.95 to 656 μg-N m⁻² day⁻¹ (Fig. 2). The highest N₂O flux during the freezing period was observed at Chamber 14 on days 31 and 70.

Relationship between N₂O flux and soil temperature or WFPS

Although a large variance occurred in the N₂O flux in the summer, the highest N₂O flux values were observed during the period with the highest soil temperature (Fig. 5). During the nonfreezing period, the 10th percentile for N₂O flux (i.e., higher than 426 μg-N m⁻² day⁻¹) was above 13.3°C in soil temperature. In addition, the highest N₂O fluxes were observed mostly in the chambers at lower positions on the slope, which also exhibited the highest WFPS values (Fig. 5).

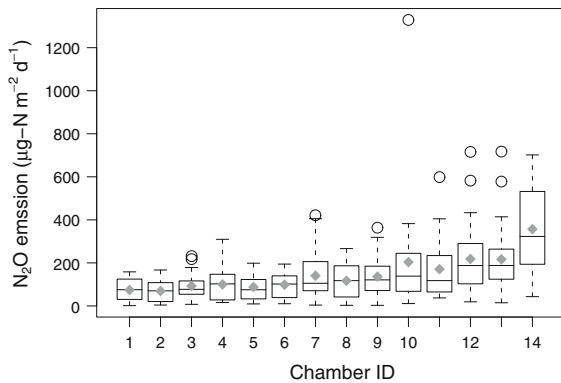


Fig. 4 Boxplot of N_2O flux at each chamber during the measurement period. The line in the box indicates the median (50% percentile) of N_2O flux at each chamber. The upper and lower borders of each box mark the means of the 25 and 75% percentiles, respectively. The whiskers (vertical lines above and below the box) show the largest and smallest observed values except for existing outliers. Open circles represent outliers if the largest (or smallest) value is larger (or smaller) than 1.5 times the box length from the 75% percentile (or 25% percentile). Solid squares indicate the mean N_2O flux in each chamber

Model parameters and evaluation

Because Gelman Rubin's convergence statistics of parameters were lower than 1.1, the parameters represented successful convergences. The mean and credible intervals (CIs) of the posterior of each parameter are summarized in Table 2.

The coefficients β_{1i} (for soil temperature) and β_{2i} (for WFPS) were always positive within the 95% CI, which indicates that both variables positively affected N_2O flux (Table 2). β_{1i} at each chamber showed a gradual increase with descending slope (Fig. 6). The 95% CI of α_{1i} and α_{2i} included 0 (Table 2). Therefore, the trend of β_{1i} along slope was not fully explained by annual mean WFPS and C/N ratio at each chamber (Table 2; Fig. 7). However, the 80th percentile of the posterior distribution of α_{2i} was marginal (-0.033 to 0.006), which indicates that the C/N ratio had a weakly negative effect on soil temperature dependency (β_{1i}).

We calculated the Q_{10} value via simulations using posterior distributions (Table 3). The median of Q_{10} varied from 1.18 to 2.64 and the highest Q_{10} was observed in Chamber 14. All Q_{10} values for each chamber exhibited large uncertainties. For example, the Q_{10} at Chamber 14 ranged from 0.49 to 19.4 with a 95% CI and 0.90–10.02 with an 80% CI.

Finally, we compared the posterior predictive N_2O flux simulated by the model with the observed N_2O flux in Fig. 8. The upper of 95% CI included high values, suggesting that the model exhibited a large uncertainty for high N_2O flux values. The simulation of N_2O flux gave good predicted values at each chamber. Most of the observed values were close to the 50% prediction line and all of the observed values fell within the 95% prediction interval (Fig. 8).

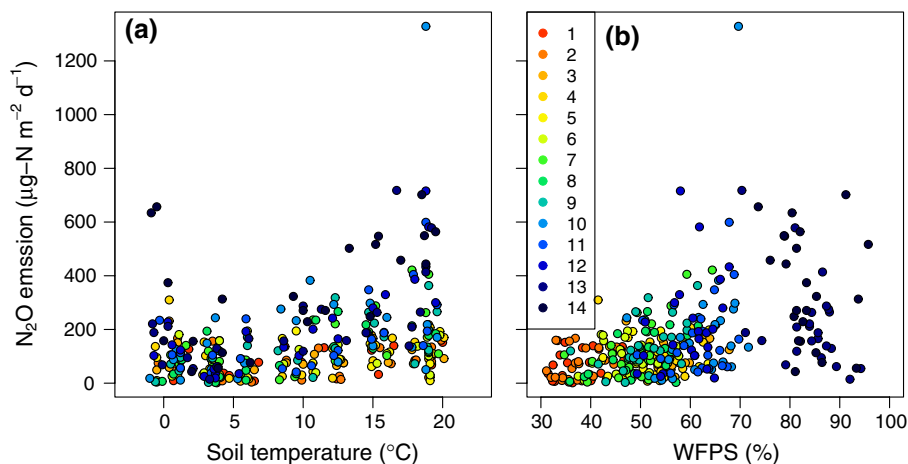


Fig. 5 Relationship between N_2O flux and soil temperature (a) and WFPS (b). Data for each chamber are distinguished by colored circles

Table 2 Summary of the posterior distribution for each parameter

Coefficients	Mean	50% (median)	95% CI	80% CI
<i>beta0</i>	2.755	2.770	1.965–3.013	2.27–3.26
<i>beta1</i> (overall) ^a	0.069	0.069	0.002–0.126	0.033–0.107
<i>beta2</i>	0.019	0.019	0.005–0.033	0.010–0.028
<i>sigma1</i>	0.813	0.812	0.743–0.835	0.77–0.858
<i>sigma1D</i>	0.167	0.148	0.062–0.381	0.08–0.273
<i>alpha0</i>	0.298	0.297	–0.319–0.918	–0.109–0.682
<i>alpha1</i>	–0.0067	–0.0007	–0.0048–0.0036	–0.0032–0.0018
<i>alpha2</i>	–0.014	–0.013	–0.044–0.017	–0.033–0.006
<i>sigma2</i>	0.051	0.049	0.033–0.083	0.037–0.067

^a *beta1* values represent as the plot scale values (Fig. 6a), which indicate marginalized over all chambers

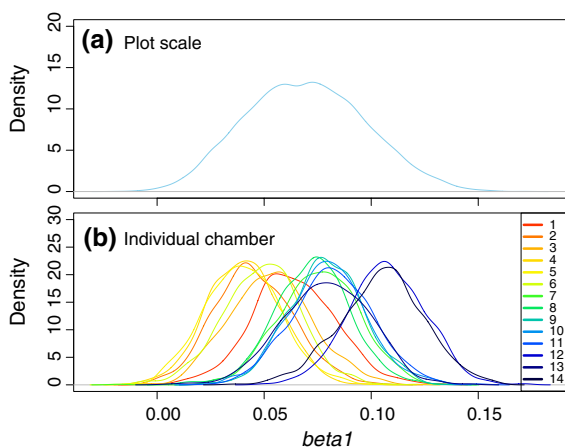


Fig. 6 Posterior distribution of *beta1* (parameter of temperature dependency) for plot scale (a) and individual chambers (b). Line color indicates chamber ID

Discussion

Spatiotemporal variation in N₂O flux during the nonfreezing period

The range in N₂O flux values at our site (1.44–1,330 μg-N m⁻² day⁻¹) was comparable to those reported by Morishita et al. (2007) in eight Japanese cedar forest sites (0–1,720 μg-N m⁻² day⁻¹). In addition, our N₂O flux values were on the same order as those in non-fertilized pine forest (144–1,272 μg-N m⁻² day⁻¹; Butterbach-Bahl et al. 1997). In comparison to N₂O fluxes recorded in European deciduous forests (e.g., 14,400 μg-N m⁻² day⁻¹; Papen and Butterbach-Bahl 1999), the maximum N₂O flux in our study was relatively low.

The spatial variations in N₂O flux followed a gradient such that more N₂O was emitted with descending position (Fig. 4). This is in accordance with previous reports (McSwiney et al. 2001; Osaka et al. 2006). For example, on the day of the highest air temperature (27°C, day 227 of the observation period), the highest N₂O flux observed at Chamber 13 (578.2 μg-N m⁻² day⁻¹) was approximately six times larger than the lowest N₂O flux at Chamber 2 (91.5 μg-N m⁻² day⁻¹). Thus, our results suggest that lower positions along a slope are more substantial sources of N₂O.

The temperature dependency of N₂O flux also gradually increased with descending slope position (Fig. 6b). The variance of each chamber's coefficient (*beta1_i*) was sufficiently smaller than that of the plot scale (overall *beta1* in Fig. 6a). This suggests that spatial information regarding slope position is important for spatial estimation of N₂O flux as it enables reduced uncertainty in the estimation of parameters (Fig. 6).

Our hierarchical model indicated that the gradient of temperature dependency along a slope was partially explained by the C/N ratio rather than annual mean WFPS (Table 2). At our study site, the C/N ratio gradually decreased with descending slope (Table 1). Hirobe et al. (1998) reported the same spatial trend in the C/N ratio along a slope of a coniferous forest, and stated that the net N mineralization and net nitrification rates were low at the shoulder due to the high C/N ratio and low water content. Therefore, a higher position along the slope might be characterized by a low concentration of substrates (i.e., NH₄⁺, NO₃⁻) for both nitrification

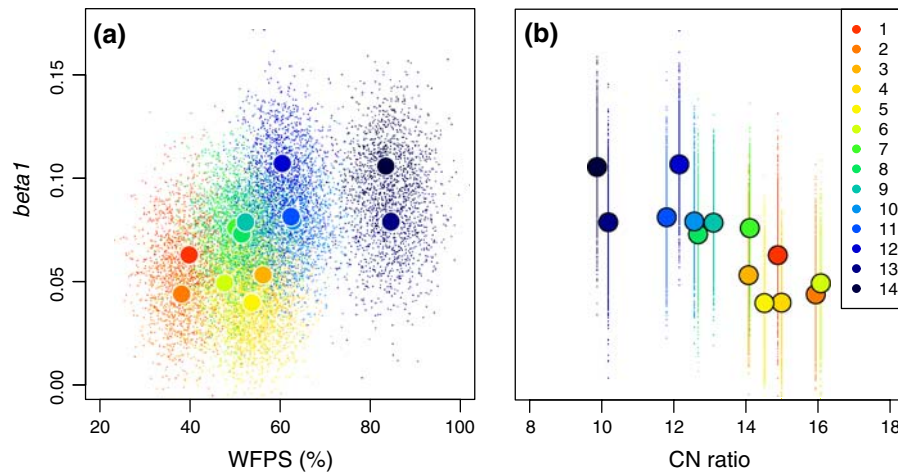


Fig. 7 Relationship between the posterior distribution of β_{1} and annual mean WFPS (a) and C/N ratio (b). Circles and dot colors indicate the chamber number. Circles denote the median value for each chamber

Table 3 Simulated Q_{10} value from the Bayesian model

Chamber ID	50.0%	95% CI	80% CI
1	1.72	0.21–10.31	0.52–5.78
2	1.58	0.23–9.96	0.50–4.94
3	1.18	0.18–8.35	0.35–4.18
4	1.30	0.22–9.31	0.39–4.40
5	1.35	0.24–10.58	0.44–4.74
6	1.70	0.25–10.29	0.51–5.47
7	2.09	0.28–11.95	0.62–6.53
8	2.06	0.29–12.28	0.60–6.78
9	1.75	0.31–10.28	0.55–5.55
10	2.32	0.36–12.34	0.73–7.30
11	2.56	0.43–16.16	0.79–8.39
12	3.64	0.58–25.65	1.10–12.88
13	2.38	0.34–15.10	0.77–7.66
14	3.03	0.49–19.40	0.90–10.02

and denitrification process. Presumably, the N_2O flux at higher positions on the slope is limited by low concentrations of substrates rather than soil temperature. In addition, the contribution of each process to N_2O emissions, which vary spatially with position along the slope (Nishina et al. 2009), might affect the spatial variability in the temperature dependency of N_2O flux. Therefore, the temperature dependency of N_2O flux was evaluated as the synthesis of these parameters. However, further research is needed to clarify response of each process to temperature for a more accurate evaluation.

The Q_{10} value is widely used as an index of the soil temperature dependency of N_2O emissions. Smith et al. (2003) suggested that the Q_{10} value of N_2O emissions reported by previous studies varied widely from approximately 2–14. In our estimation, the median of Q_{10} values for each chamber simulated from the posterior distribution ranged from 1.18 to 3.64, which is comparable with the Q_{10} range of from 2 to 4 reported for typical biological reactions (Castaldi 2000). However, the simulated Q_{10} exhibited a large uncertainty (Table 3), likely because the posterior distribution of N_2O flux had a large upper interval, especially in the high temperature range. This was due to a characteristic of the error term of a lognormal distribution, which is proportional to an increased scale parameter (e.g., Fig. 8). Indeed, occasional high N_2O fluxes were observed in our study, especially at high temperatures (e.g., on day 206 at Chamber 10; Figs. 3, 8). This was also observed in many previous studies (e.g., von Arnord et al. 2005a, b; Morishita et al. 2007). In our lognormal distribution model, the probability of observing extreme high N_2O flux becomes more likely (Fig. 8). In addition, the estimation of Q_{10} calculated by the exponential function often exhibited a large uncertainty, especially if the regression coefficient was low. However, this kind of uncertainty is not considered in traditional models.

In some previous reports, an occasional high N_2O flux often reduced the accuracy of linear regression models for estimating N_2O flux because the high

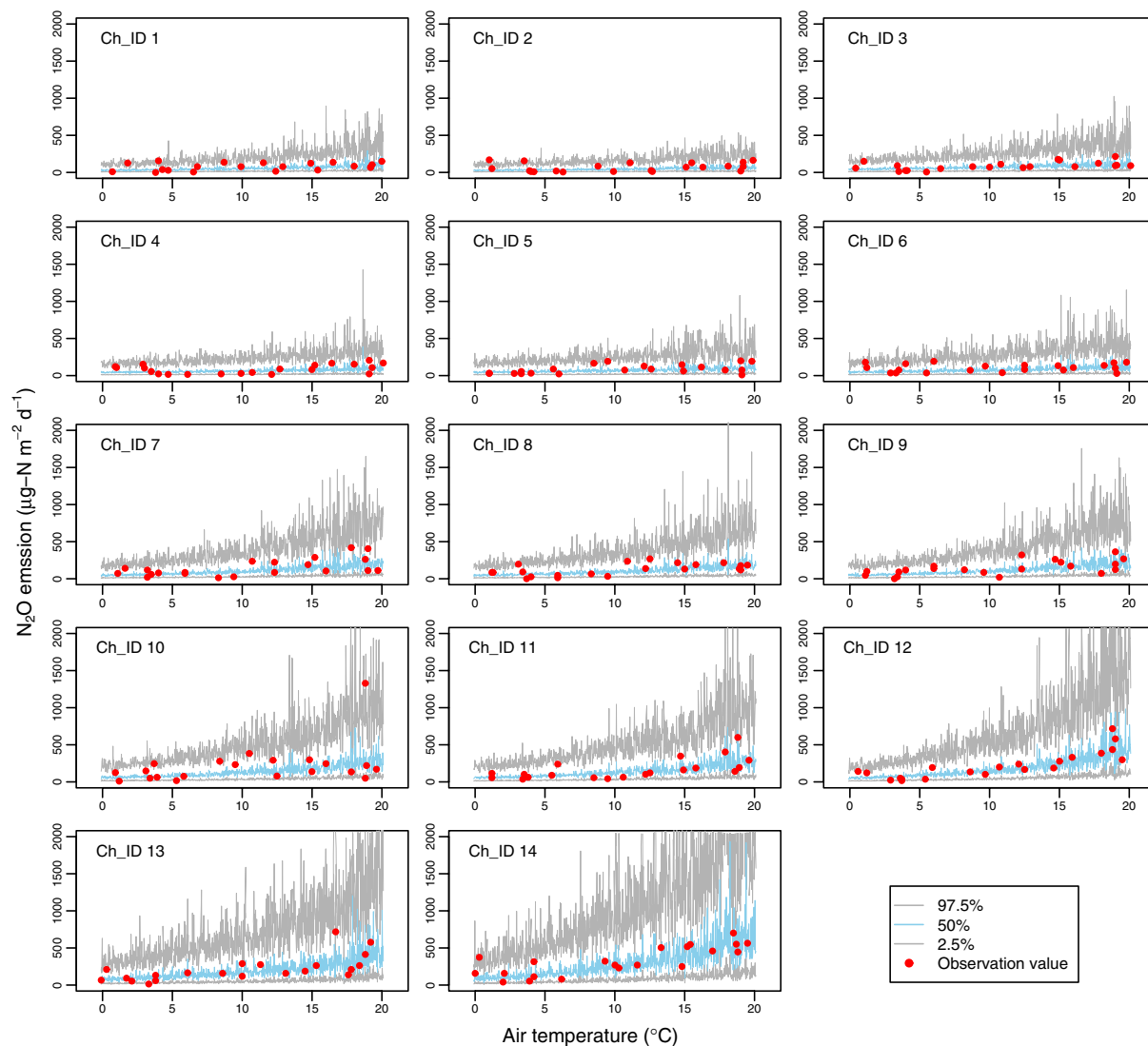


Fig. 8 Observed and simulated probabilities of N_2O flux (during nonfreezing periods). *Solid circles* indicate observed N_2O fluxes. Simulated probabilities are presented by the 50% line (median; blue line) with a 95% prediction interval (gray line)

values were not explained by a single factor or combination of parameters such as temperature, water conditions, and nitrate concentration (e.g., von Arnord et al. 2005a; Tang et al. 2006; Adviento-Borbe et al. 2007). This type of occasional high N_2O flux in summer could be partly explained by the development of an anaerobic zone in the soil (Smith 1997). Smith (1997) suggested that such a zone would contribute to N_2O emissions from soil aggregates as a result of stimulation by a reduction in oxygen caused by the high activity of microorganisms due to increased temperature. In situ, the soil

aggregates contributing to N_2O emissions might not be uniformly distributed even if the WFPS is consistent. It is possible that this condition occurs not entirely randomly but with a weak definite relation to WFPS and other environmental factors. However, we could not adequately monitor the detailed oxidative condition of the soil. In addition, high N_2O fluxes occurred infrequently, suggesting that this kind of N_2O emission is hardly observed. To model infrequently high N_2O flux, our Bayesian hierarchical model accounted for this problem by treating the occasional high N_2O emission as the error

term of the lognormal distribution. We overcame the second problem by simultaneously modeling the individual chamber's flux and that of the plot scale (overall data) using a Bayesian hierarchical model with CAR. For example, the upper 95% predictive interval of chamber 8 was much higher than the observed flux values (Fig. 8). This is because the estimation of parameters for Chamber 8 is shrunken to the estimation parameters of the plot scale. This complementary use of information in the Bayesian model enabled plausible estimations of the effects of environmental factors on highly skewed spatiotemporal N₂O flux data.

N₂O flux during the soil freezing period

Relatively high N₂O emissions were observed during the freezing period (days 31 and 70) in some chambers. For example, the N₂O flux in Chamber 14 at day 31 was 656 $\mu\text{g-N m}^{-2} \text{ day}^{-1}$, which is six times higher than the median of the whole N₂O flux value in this study. Conversely, no high N₂O emissions were observed during thawing period (days 58 and 88) in any chambers. Papen and Butterbach-Bahl (1999) and Teepe et al. (2000) also reported relatively high N₂O emissions from frozen forest soils. Teepe et al. (2001) described an occurrence of relatively high N₂O emissions under freezing soil conditions compared to thaw periods using incubation experiments. This was due to a denitrification process that occurs in unfrozen water in frosty soil (Teepe et al. 2001). Specifically, accumulations of dead organisms from freezing produce an abundant labile carbon source in the unfrozen water (Yanai et al. 2004). In addition, NO₃⁻ concentrations in unfrozen water are thought to increase as a result of condensation by freezing (Teepe et al. 2001), and the ice layer suppresses the oxygen supply. Thus, frosty soil is important site of N₂O emissions during freezing periods.

Our results demonstrated that the N₂O flux during the freezing period varied spatially along the slope. The highest N₂O flux on both soil-freezing days was observed in the chamber located at the foot slope (Chamber 14; Fig. 2a). The frost depth at the foot slope was deeper than that at the shoulder. Although the frost depth differed markedly between days 31 and 70, no substantial difference in N₂O emissions

occurred between these days. Maljanen et al. (2007) reported that the N₂O emissions at deeper soil freezing point (100 cm) after the removal of snow cover was greater than those at shallower soil freezing points (20 cm) on agricultural soil. The freezing depth in our study site (maximum 14 cm) was shallower than those examined by Maljanen et al. (2007). Therefore, the effect of freezing depth on N₂O emissions might be relatively weaker in our study. Little published information is available on controlling factors affecting N₂O emissions during freezing periods (Teepe et al. 2004). Thus, we were unable to thoroughly monitor these factors or to statistically model the N₂O flux during the freezing period. Groffman et al. (2001) suggested that soil freezing has become an increasingly important factor in N₂O emissions because of the reduction in snow insulation due to global warming. To assess the distribution and contribution of N₂O emissions during freezing periods to the annual N₂O budget, a more accurate understanding of the controlling factors and mechanisms is essential.

Conclusions

Our results revealed spatiotemporal variation of N₂O fluxes along a slope of Japanese cedar forest. High spatial and temporal variations in N₂O flux were observed along the slope for 1 year. The N₂O fluxes at the foot slope were relatively higher than at the top of the slope. Furthermore, the soil temperature sensitivity of the N₂O flux exhibited the spatial trend of increasing with descending slope. Our results indicated that spatial information regarding topographic factors would help reduce the uncertainty in estimating N₂O flux. In addition, this trend of spatial soil temperature dependency along a slope was partially explained by the C/N ratio of surface soils. We successfully modeled the spatiotemporal N₂O flux and quantified the effect of environmental factors on the N₂O flux with taking account for uncertainty using a hierarchical Bayesian model with CAR, which is a more statistically adequate model than traditional approaches. Finally, our results confirmed that N₂O fluxes during freezing periods exhibit spatial variation and that they constitute important contributions to the N₂O budget in Japanese coniferous forests.

Acknowledgments We are grateful to the staff of the Nagoya University experimental forest, especially Mr. Y. Imaizumi, Mr. N. Yamaguchi, and Mr. N. Takabe, for their support. We thank Dr. T. Yoshida for his valuable comments and help with sampling, and Dr. I. Tamaki for his valuable comments regarding statistical modeling.

References

- Adviento-Borbe MAA, Haddix ML, Binder DL, Walters DT, Dobermann A (2007) Soil greenhouse gas fluxes and global warming potential in four high-yielding maize system. *Global Change Biol* 13:1972–1988
- Besag J, York JC, Molife A (1991) Bayesian image restoration with two applications in spatial statistics (with discussion). *Ann Inst Stat Math* 43:1–59
- Brumme R (1995) Mechanism of carbon and nutrient release and retention in beech forest gaps. *Plant Soil* 168–169:593–600
- Butterbach-Bahl K, Gasche R, Breuer L, Papen H (1997) Fluxes of NO and N₂O from temperate forest soils: impact of forest type, N deposition and of liming on the NO and N₂O emissions. *Nutr Cycl Agroecosyst* 48:79–90
- Castaldi S (2000) Responses of nitrous oxide, dinitrogen and carbon dioxide production and oxygen consumption to temperature in forest and agricultural light-textured soils determined by model experiment. *Biol Fertil Soil* 32: 67–72
- Clark JS (2005) Why environmental scientists are becoming Bayesians. *Ecol Lett* 8:2–14
- Crutzen PJ (1995) Ozone in the troposphere. In: Sing HB (ed) *Composition, chemistry and climate of the atmosphere*. Van Nostrand Reinhold Publ, New York, pp 349–393
- Danielson RE, Sutherland PL (1986) Porosity. In: Kulute A (ed) *Method of soil analysis, part I—physical and mineralogical methods*, 2nd edn. Soil Science Society of America, Madison, WI, pp 443–461
- Davidson EA, Ishida FY, Nepstad DC (2004) Effect of an experimental drought on soil emission of carbon dioxide, methane, nitrous oxide, and nitric oxide in a moist tropical forest. *Global Change Biol* 10:718–730
- Gelfand AE, Latimer A, Wu S, Silander JA Jr (2005) Building statistical models to analyze species distribution. In: Clark JE, Gelfand AE (eds) *Hierarchical modeling for the environmental sciences, statistical methods and applications*. Oxford University Press, Oxford, pp 76–97
- Groffman PM, Driscoll CT, Fahey TJ, Hardy JP, Fitzhugh RD, Tierney GL (2001) Colder soils in a warmer world: a snow manipulation study in a northern hardwood forest ecosystem. *Biogeochemistry* 56:135–150
- Hardy JP, Groffman PM, Fitzhugh RD, Henry KS, Welman AT, Demers JD, Fahey TJ, Driscoll CT, Tierney GL, Nolan S (2001) Snow depth manipulation and its influence on soil frost and water dynamics in a northern hardwood forest. *Biogeochemistry* 56:151–174
- Hawkins MJ, Hyde BP, Ryan M, Schulte RPO, Connolly J (2007) An empirical model and scenario of nitrous oxide emissions from a fertilized and grazed grass land site in Ireland. *Nutr Cycl Agroecosyst* 79:93–101
- Hirobe M, Tokuchi N, Iwatubo G (1998) Spatial variability of soil nitrogen transformation patterns along a forest slope in *Cryptomeria japonica* D. Don plantation. *Eur J Soil Biol* 34:123–131
- Hutchinson GL, Mosier A (1981) Improved soil cover method for field measurement of nitrous oxide fluxes. *Soil Sci Soc Am J* 45:311–316
- IPCC (2001) *Climate change 2001: the scientific basis*. International panel on climate change. Cambridge University Press, Cambridge, UK
- Ishizuka S, Sakata T, Ishizuka K (2000) Methane oxidation in Japanese forest soils. *Soil Biol Biochem* 32:769–777
- Ishizuka S, Iswandi A, Nakajima Y et al (2005) Spatial patterns of greenhouse gas emission in a tropical rainforest in Indonesia. *Nutr Cycl Agroecosyst* 71:55–62
- Konda R, Ohta S, Ishizuka S, Arai S, Ansori S, Tanaka N, Hardjono A (2008) Spatial structures of N₂O, CO₂ and CH₄ fluxes from *Acacia mangium* plantation soils during a relatively dry season in Indonesia. *Soil Biol Biochem* 40:3021–3030. doi:10.1016/j.soilbio.2008.08.022
- Lark RM, Milne AE, Addiscott TM, Goulding KWT, Webster CP, O’Flaherty S (2004) Scale- and location-dependent correlation of nitrous oxide emissions with soil properties: an analysis using wavelets. *Eur J Soil Sci* 55:611–627
- Maag M, Vinther FP (1996) Nitrous oxide emission by nitrification and denitrification in different soil types and at different soil moisture contents and temperatures. *Appl Soil Ecol* 4:5–14
- Maljanen M, Kohonen AR, Virkajarvi P, Martikainen PJ (2007) Fluxes and production of N₂O, CO₂ and CH₄ in boreal agricultural soil during winter as affected by snow cover. *Tellus* 59B:853–859
- McSwiney CP, McDowell WH, Keller M (2001) Distribution of nitrous oxide and regulator of its production across a tropical rainforest catena in the Luquillo Experimental Forest, Puerto Rico. *Biogeochemistry* 56:265–286
- Morishita T, Sakata T, Takahashi M et al (2007) Methane uptake and nitrous oxide emission in Japanese forest soils and their relationship to soil and vegetation types. *Soil Sci Plant Nutr* 53:678–691
- Mosier AR (1998) Soil processes and global change. *Biol Fertil Soils* 27:221–229
- Nishina K, Takenaka C, Ishizuka S (2009) Spatial variations in nitrous oxide and nitric oxide emission potential on a slope of Japanese cedar (*Cryptomeria japonica*) forest. *Soil Sci Plant Nutr* 55:179–189. doi:10.1111/j.1747-0765.2007.00315.x
- Osaka K, Ohte N, Koba K, Katsuyama M, Nakajima T (2006) Hydrologic controls on nitrous oxide production and consumption in a forested headwater catchment in central Japan. *J Geophys Res* 111:G01013. doi:10.1029/2005JG000026
- Papen H, Butterbach-Bahl K (1999) A 3-year continuous record of nitrogen trace gas fluxes from untreated and limed soil of a N-saturated spruce and beech forest ecosystem in Germany 1. N₂O emissions. *J Geophys Res* 104:18487–18503
- Parkin TB, Robinson JA (1989) Stochastic models of soil denitrification. *Appl Environ Microbiol* 55:72–77
- Schoeneberger PJ, Wysocki DA, Benham EC, Broderson WD (1998) *Field book for describing and sampling soils*. U.S.

- Department of Agriculture, Natural Resources Conservation Service, National Soil Survey Center, Lincoln, NE
- Smith KA (1997) The potential for feedback effects induced by global warming on emissions of nitrous oxide by soils. *Global Change Biol* 3:327–338
- Smith KA, Thomson PE, Clayton H, McTaggart IP, Conen F (1998) Effect of temperature, water content and nitrogen fertilization on emissions of nitrous oxide by soils. *Atmos Environ* 32:3301–3309
- Smith KA, Ball F, Conen KE, Dobbie KE, Massheder J, Rey A (2003) Exchange of greenhouse gases between soil and atmosphere: interactions of soil physical factors and biological processes. *Eur J Soil Sci* 54:779–791
- Spiegelhalter DTA, Best N (2000) WinBUGS user manual. MRC Biostatistics Unit, Cambridge, UK
- Stow CA, Recknow KH, Qian SS (2006) A Bayesian approach to retransformation bias in transformed regression. *Ecology* 87:1472–1477
- Tang X, Liu S, Zhou G, Zhang D, Zhou C (2006) Soil atmospheric exchange of CO₂, CH₄ and N₂O in three subtropical forest ecosystems in southern china. *Global Change Biol* 12:546–560
- Teepe R, Brumme R, Beese F (2000) Nitrous oxide emissions from frozen soils under agricultural, fallow and forest land. *Soil Biol Biochem* 32:1807–1810
- Teepe R, Brumme R, Beese F (2001) Nitrous oxide emissions from soil during freezing and thawing periods. *Soil Biol Biochem* 33:1269–1275
- Teepe R, Vor A, Beese F, Ludwig B (2004) Emissions of N₂O from soils during cycles of freezing and thawing and the effect of soil water, texture and duration of freezing. *Eur J Soil Sci* 55:357–365
- USDA-NRCS (1999) Soil taxonomy, 2nd edn. <http://soils.usda.gov/technical/classification/taxonomy/>
- Velthof GL, Jarvis SC, Stein A, Allen AG, Oenema O (1996) Spatial variability of nitrous oxide fluxes in mown and grazed grasslands on a poorly drained clay soil. *Soil Biol Biochem* 28:1215–1225
- von Arnord K, Ivarsson M, Oqvist M, Majdi H, Bjork RG, Weslien P, Klemedtsson L (2005a) Can distribution of trees explain variation in nitrous oxide fluxes? *Scand J For Res* 20:481–489
- von Arnord K, Nilsson M, Hanell B, Weslien P, Klemedtsson L (2005b) Fluxes CO₂, CH₄ and N₂O from drained organic soils in deciduous forest. *Soil Biol Biochem* 37: 1059–1071
- Yanai Y, Toyota K, Okazaki M (2004) Effects of successive soil freeze thaw cycles on soil microbial biomass and organic matter decomposition potential of soils. *Soil Sci Plant Nutr* 50:821–829
- Yoshida T, Hijii N (2006) Spatiotemporal distribution of aboveground litter in a *Cryptomeria japonica* plantation. *J For Res* 11:419–426